The Journal of Immunology
RESEARCH ARTICLE | JUNE 15 2021

Selective Activation of MST1/2 Kinases by Retinoid Agonist Adapalene Abrogates AURKA-Regulated Septic Arthritis

Preeti Yadav; ... et. al

J Immunol (2021) 206 (12): 2888–2899.
https://doi.org/10.4049/jimmunol.2001360

Selective Activation of MST1/2 Kinases by Retinoid Agonist Adapalene Abrogates AURKA-Regulated Septic Arthritis

Preeti Yadav, Bharat Bhatt, and Kithiganahalli Narayanaswamy Balaji

Septic arthritis is a chronic inflammatory disorder caused by *Staphylococcus aureus* invasion of host synovium, which often progresses to impairment of joint functions. Although it is known that disease progression is intricately dependent on dysregulated inflammation of the knee joint, identification of molecular events mediating such imbalance during *S. aureus*–induced septic arthritis still requires detailed investigation. In this article, we report that Aurora kinase A (AURKA) responsive WNT signaling activates *S. aureus* infection–triggered septic arthritis, which results in inflammation of the synovium. In this context, treatment with adapalene, a synthetic retinoid derivative, in a mouse model for septic arthritis shows significant reduction of proinflammatory mediators with a simultaneous decrease in bacterial burden and prevents cartilage loss. Mechanistically, adapalene treatment inhibits WNT signaling with concomitant activation of HIPPO signaling, generating alternatively activated macrophages. Collectively, we establish adapalene as a promising strategy to suppress *S. aureus*–induced irreversible joint damage. *The Journal of Immunology*, 2021, 206: 2888–2899.

Septic arthritis is a severe purulent inflammatory disease that results from colonization of invasive infectious microbes, majorly bacteria, in joints. Among invasive bacterial infections, *Staphylococcus aureus* accounts for 37–67% of clinical isolates from septic arthritis cases among various categories of patients (1, 2). Limited antibiotic treatment, as well as increased antibiotic resistance to *S. aureus*, limits various options in terms of curtailing invasive infections like endocarditis (3), bacteraemia (4), and osteomyelitis (5).

In the context of septic arthritis, clinically proven disease-modifying antirheumatic drugs that are in clinical utility assume important roles in modulating hyperinflammation to prevent immune system dysregulations (6). However, in many cases, treatment of septic arthritis among patients becomes ineffective, owing to the development of refractoriness not only to disease-modifying antirheumatic drugs but to various biologics and biosimilars, as well (7). In this regard, vitamin A metabolite, retinoic acid (RA), is shown to potentiate anti-inflammatory T regulatory (Treg) cell expansion (8). Moreover, zymogen-driven RA induction results in dendritic cell–mediated Foxp3$^+$ T cell expression and elevated SOCS3 level with concomitant reduction of proinflammatory cytokines (9). Importantly, RA is documented in the amelioration of collagen-induced arthritis, which helps in improving the clinical symptoms of an autoimmune disorder (10). However, a direct role for RA, if any, on curtailing bacterial-induced septic arthritis development has not yet been investigated. In this perspective, we explored whether a synthetic derivative of RA (adapalene [ADA], a biologically active and key metabolite of vitamin A) would suppress *S. aureus*–triggered septic arthritis. ADA is a third-generation RA receptor (RAR-β,γ) selective agonist, approved by the U.S. Food and Drug Administration (FDA) with a broad safety profile, and it is chemically stable (FDA identifier 090962). It is an established comedolytic and efficacious chemotherapeutic agent (11) that has never been explored against bacterial sepsis. Our current investigation demonstrates that ADA regulates key signaling events involved in *S. aureus*–elicited septic arthritis in mice. Specifically, NOD2-mediated activation of AURKA–WNT signaling during *S. aureus* infection is found to activate proinflammatory chemokines, culminating in the development of septic arthritis. Administration of ADA inhibited both onset and development of septic arthritis through suppression of WNT signaling. In line with this, ADA-induced HIPPO signaling potentiated anti-inflammatory macrophage phenotype and mounted proresolvin E1 receptor CHEMR23 expression, thereby leading to the abrogation of septic arthritis development. Together, this study establishes ADA as a preventive intervention for *S. aureus*–driven septic arthritis.

Materials and Methods

Mice, cells, and bacteria

BALB/c mice were purchased from The Jackson Laboratory and maintained in the Central Animal Facility, Indian Institute of Sciences, Bangalore, India. Mice were i.p. injected with 8% Brewer thioglycollate and sacrificed after

Department of Microbiology and Cell Biology, Indian Institute of Science, Bangalore, Karnataka, India

Received for publication December 3, 2020. Accepted for publication April 4, 2021.

This work was supported by funds from the Department of Biotechnology, Ministry of Science and Technology, India (DBT) (BT/PR13522/COE/34/27/2015 and BT/PR27352/BRB/10/1639/2017), and the Department of Science and Technology, Ministry of Science and Technology, India (DST) (EMR/2014/000875). This work was also supported by a J. C. Bose National Fellowship award (SB/S2/JCB-025/2016) and CRG/2019/002062 funding to K.N.B. Funding and infrastructure support was provided by the DST–Fund for Improvement of S&T Infrastructure, the University Grants Commission (UGC) Centre for Advanced Study, and the DBT–Indian Institute of Science (IISc) Partnership Program (Phase II at IISc, BT/PR27952/INF/22/212/2018). Fellowship assistance from the Council of Scientific and Industrial Research (to P.Y.) and UGC (to B.B.) was provided.

P.Y. and K.N.B. conceived and designed the study. P.Y. and B.B. performed the experiments and analyzed the data. P.Y. and K.N.B. wrote the paper.

Address correspondence and reprint requests to Dr. Kithiganahalli Narayanaswamy Balaji, SE-14, Department of Microbiology and Cell Biology, Indian Institute of Science, Bangalore 560012, Karnataka, India. E-mail address: balaji@iisc.ac.in

The online version of this article contains supplemental material.

Abbreviations used in this article: ADA, adapalene; FDA, U.S. Food and Drug Administration; Fwd, forward; MOI, multiplicity of infection; RA, retinoic acid; Rvs, reverse; siRNA, small interfering RNA; Treg, T regulatory.

4 d to isolate peritoneal macrophages via gastric lavage with ice-cold PBS. Isolated cells were cultured in DMEM containing 10% FBS for 12 h, and adherent cells were used as peritoneal macrophages. Murine RAW264.7 macrophage cell line was obtained from the National Centre for Cell Sciences, Pune, India. *S. aureus* Cowan 1 (Microbial Type Culture Collection identifier 902) was obtained from the Microbial Type Culture Collection, Institute of Microbial Technology, Chandigarh, India.

Ethics statement

All studies involving mice were carried out after approval from the institutional ethics committee as well as from the institutional biosafety committee. Animal handling, care, and use protocols were approved by the national guidelines of the Committee for the Purpose of Control and Supervision of Experiments on Animals, Government of India.

Reagents and Abs

DMEM and FBS were purchased from Life Technologies–Invitrogen/Thermo Fisher Scientific. Anti-β-ACTIN (A3854) Ab was purchased from Sigma-Aldrich. Anti-Ser-33/37/Thr-41 phospho-β-CATENIN (9561), anti-β-CATENIN (9562), anti-Ser-9 phospho-GSK-3β (9322), anti-GSK-3β (9315), anti-Thr-288 phospho-AURORA KINASE A (3079), anti-AURORA KINASE A (3092), anti-Ser-2448 phospho mTOR (2971), anti-mTOR (2972), anti-Thr-1079 phosphor-LATS1 (8654), anti-LATS-1 (3477), anti-Thr-183 Phopho-MST1/Thr-180MST2 (3681), anti-MST1 (14946), anti-MST2 (3952), anti–IL-1β (12242), and anti-ARGINASE1 (9819) Abs were obtained from Cell Signaling Technology. Anti-CHEMR23 (ab64881) was purchased from Abcam. HRP-conjugated anti-rabbit IgG Ab (111-035-045) and anti-mouse Alexa 647 (715-605-151) were purchased from Jackson ImmunoResearch. Anti-CD11b FITC (101205), anti-CD64 PE/Cy7 (139313), and anti-rabbit Alexa 647 (406414) were purchased from BioLegend. BV510 live/dead dye (13-0870) was purchased from Tonbo Biosciences. Nontargeting small interfering RNA (siRNA) (D-001210-01-20) and *Stk4*/*Mst1* (M-059385-01-0005) and *Stk3*/*Mst2* (M-040440-01-0005) siRNAs were obtained from Dharmacon as siGENOME SMARTpool reagents.

Treatment with pharmacological reagents

In all experiments involving pharmacological reagents, a titrated concentration was used after assessing viability of the macrophages using trypan blue assay. In all in vitro experiments, peritoneal macrophages were pretreated for 1 h with inhibitors at the following concentrations: alisertib (1 μM) (1028486-01-2; Cayman), rapamycin (100 nM) (553210; Calbiochem), and ADA (5 μM) (114825; Calbiochem).

In vitro *S. aureus* infection

S. aureus was grown in Luria Broth at 37°C until the OD_{600} reached 0.2, corresponding to $\sim 1 \times 10^7$ CFU per milliliter. Bacteria were harvested, washed with PBS, and resuspended in cell culture complete DMEM without antibiotics. Peritoneal macrophages were infected with *S. aureus* at a multiplicity of infection (MOI) of 1:10.

Intra-articular infection of mice

For in vivo experiments, mice were anesthetized with a single dose of ketamine (120 mg/kg) and xylazine (16 mg/kg) mixture. Hind limbs were shaved, and the left knee was intra-articularly injected with live *S. aureus.* The right knee was injected with PBS as vehicle control. Mice were monitored for the next 7 d for limping and restricted hind limb movement.

RNA isolation and quantitative real-time RT-PCR

For in vivo studies, the whole hind limb tissue was pulverized based on a previously established protocol (12, 13). Briefly, the outer skin of the hind limb from *S. aureus*–infected or ADA-treated mice was removed, and the whole joint (including synovial tissue, ligaments, and bone) was crushed in a precooled mortar and pestle in liquid nitrogen. Finely minced tissue was collected. Crushed tissue or treated macrophages, as indicated, from in vitro experiments were subjected to total RNA isolation using TRI reagent (T9424; Sigma-Aldrich). RNA was used for cDNA synthesis using first-strand cDNA synthesis kit (M3682; Promega). Quantitative real-time PCR was performed with SYBR green PCR mix (RR420A; Takara) in an ABI machine. All experiments were repeated in biological triplicate with technical duplicates taken in each experiment to ensure reproducibility of data. Mean cycle threshold values were normalized to internal control *Gapdh*. Primers used for quantitative real-time PCR are as follows: *Gapdh* forward (Fwd) 5′-gagccaaacgggtcatcatct-3′, reverse (Rvs) 5′-gaggggccatccacagtctt-3′; *Cxcl1* Fwd 5′-tgttgtgcgaaa agaagtgc-3′, Rvs 5′-cgagacgagaccaggagaaa-3′; *Il-1β* Fwd 5′-ga aatgccacctttgacagtg-3′, Rvs 5′-tggatgctctcatcaggacag-3′; *Ccl2* Fwd 5′-taaaaacctggatcggaaccaaa-3′, Rvs 5′-gcattagcttcag atttacgggt-3′; *Ccl4* Fwd 5′-aaacctaaccccgagcaaca-3′, Rvs 5′-ccattggtgctgagaaccct-3′; *Ccl5* Fwd 5′-ccct caccatcatcctcact-3′, Rvs 5′-ccttcgagtgacaaacacga-3′; *Ccl11* Fwd 5′-cagatgcaccc tgaaagccata-3′, Rvs 5′-tgctttgtggcatcctgga-3′; *Ccl12* Fwd 5′-atttccacacttctatg cctcct-3′, Rvs 5′-atccagtatggtcctgaagatca-3′; *Cxcl11* Fwd 5′-aggaaggtcacagccatagc-3′, Rvs 5′-cgatctctgccattt tgacg-3′; *Tnf-α* Fwd 5′-agcccacgtcgtagcaaaccaccaa-3′, Rvs 5′-acacccattcccttcacagagcaat-3′; *Nos2* Fwd 5′-ggagtgacggcaaa catgact-3′, Rvs 5′-tcgatgcacaactgggtgaac-3′; *Retnla* Fwd 5′-cc ctccactgtaacgaagactc-3′, Rvs 5′-cacacccagtagcagtcatcc-3′; *Ccl22* Fwd 5′-tgccatcacgtttagtga agg-3′, Rvs 5′-cggcaggattttgaggtcca-3′; *Ucp-1* Fwd 5′-gtgaaggtcagaatgca agc-3′, Rvs 5′-aggg ccccctcatgaggtc-3′; *Cx3cr1* Fwd 5′-cagcatcgaccggtaccttt-3′, Rvs 5′-gctgcactgtccggttgtt-3′; *Rarβ2* Fwd 5′-gcagcaccggcatactgctc-3′, Rvs 5′-ctagcccgatgacttgtcctg-3′; *Tgf-β* Fwd 5′-ccctatatttggagcctgga-3′, Rvs 5′-gttggttgtagagggcaagg-3′; *Il-10* Fwd 5′-ggactttaagggttacttggg ttgcc-3′, Rvs 5′-cattttgatcatcatgtatgcttct-3′; and *Arginase1* Fwd 5′-gtgaagaacccacggtctgt-3′, Rvs 5′-ctggttgtcaggggagtgtt-3′.

Immunoblotting

Treated macrophages, as indicated, were washed with ice-cold PBS, and collected pellet was lysed in RIPA buffer constituted of 50 mM TRIS-HCl (pH 7.4); 1% Nonidet P-40; 0.25% sodium deoxycholate; 150 mM NaCl; 1 mM EDTA; 1 mM PMSF; 1 μg/ml each of aprotinin, leupeptin, and pepstatin; 1 mM Na3VO4; and 1 mM NaF. Total protein was quantitated through Bradford method. An equal amount of protein from each sample was resolved on a 12% SDS-polyacrylamide gel and transferred to polyvinylidene difluoride membranes (IPVH00010; Millipore) by the semidry transfer (170-3940; Bio-Rad) method. To block nonspecific binding, blots were blocked with 5% skimmed milk powder in TBST (20 mM TRIS-HCl [pH 7.4]), 137 mM NaCl, and 0.1% Tween 20 for 60 min. Blots were incubated overnight at 4°C with primary Ab, followed by incubation with HRP-conjugated secondary Ab in 5% BSA for 4 h. After washing in TBST, immunoblots were developed with an ECL detection system (NEL105001EA; Perkin Elmer) as per the manufacturer's instructions. β-ACTIN was used as a loading control. To probe another protein in the same region, blots were further stripped in stripping buffer (62.5 mM TRIS-HCl [pH 6.8], 2% SDS, and 0.7% β-mercaptoethanol) at 60°C on a shaker, followed by blocking with 5% skimmed milk powder and probed with Abs as mentioned above.

Transient transfection

Peritoneal macrophages from mice were transiently transfected with 100 nM targeted siRNA for 8 h, using low-m.w. polyethyleneimine (40872-7; Sigma-Aldrich). Further 36-h posttransfection cells were treated or infected as indicated for the required time and processed for analysis.

Micro–computed tomography and its parameters

Scanned limbs covering a region of 8 mm were reconstructed into a three-dimensional structure with XRADIA XRM 500. Scanning was done at 100 kV, 89.3 μA, and 9 W with LE1 source filter. Exposure time was 1 s with a pixel size of 10.91 obtained at 1× objective with 1031 slices. Images were analyzed using AVIZO software through manual thresholding and segmentation. Analysis was performed based on set guidelines for assessment of bone microstructure in rodents (14). Parameters that were measured included bone volume/total volume, which indicates the ratio of segmented bone volume to total volume of the region of interest; trabecular thickness (millimeters), indicating the mean thickness of trabeculae; trabecular number (per millimeter), indicating a measure of the average number of trabeculae per unit length; and trabecular space volume (millimeters cubed), indicating the mean volume of the space between trabeculae.

Immunohistochemistry

Tissue sections (5 μm) obtained from decalcified and paraffin-embedded blocks were subjected to deparaffinization and rehydration. For Ag retrieval, sections were kept in 10 mM sodium citrate buffer (pH 6) for 15 min at boiling temperature. A total of 1% H_2O_2 was used to inhibit =endogenous tissue peroxidase activity, followed by blocking with 2% BSA for 1 h. These sections were incubated with primary Abs (1: 100) made in 1% BSA and 1% Tween 20 solution overnight at 4°C. After incubating with secondary anti-rabbit HRP-conjugated Ab for 6 h at 4°C, sections were stained with 0.1% diaminobenzidine (Sigma-Aldrich) in 1% H_2O_2 solution. Slides were washed with PBS counterstained with hematoxylin, dehydrated with ethanol, and mounted on DPX (Thermo Fisher Scientific product code 18404).

Histopathological examination and scoring

Tissue sections (5 μm) obtained through brief fixation in 4% formaldehyde for bone decalcification were paraffin embedded and stained with H&E. Double-blinded scoring was performed, including pathologist to analyze the severity of arthritis. Histological examination was performed based

on parameters discussed in the published report (15). Briefly, synovial inflammation was scored as 0 = normal; 1 = minimal infiltration of inflammatory cells in periarticular tissue; 2 = mild infiltration; 3 = moderate infiltration, with moderate edema; 4 = marked infiltration, with marked edema; and 5 = severe infiltration, with severe edema. Cartilage damage and bone erosion were scored as 0 = normal, 1 = minimal (minimal to mild loss of cartilage and bone), 2 = mild (mild loss of cartilage and bone), 3 = moderate (moderate loss of cartilage and bone), 4 = marked (marked loss of cartilage and bone), and 5 = severe (severe diffuse loss of cartilage and bone).

Isolation of synovial tissue to perform immunofluorescence and flow cytometry

For in vivo tissue imaging, synovial tissue from mice was isolated, as previously described (16, 17). Briefly, a midline skin incision was performed to expose knee joints. Transverse resection of the quadriceps was done at the middle, followed by distally reversing the tissue, which exposed the synovium, patella, and patellar ligament, and thus subsequently, the synovial tissue was isolated. For immunofluorescence, cryosections of 5 μm were stained with primary Abs followed by secondary Ab with DAPI for nuclei staining and imaged using Zeiss LSM 710 Meta Confocal Laser Scanning Microscope. For flow cytometry, resected synovial tissue was digested in RPMI medium (collagenase type IV [5 mg/ml], TC214; HiMedia) and DNase 1 (0.1 mg/ml, EN0521; Thermo Fisher Scientific) for 60 min at 37°C. Minced tissue was filtered through a 70-μm cell strainer and washed with FACS buffer (2% FBS with 1 mM EDTA in PBS). The single cells obtained were preincubated for 1 h with 5 μg/ml brefeldin A (Sigma-Aldrich) and stained with CD64-PECy7, CD11b-FITC, and BV510 ghost live/dead dye. For intracellular staining, cells fixed in 2% PFA were washed in FACS buffer and incubated with IL-1β and ARGINASE 1 Ab in permeabilization buffer for 60 min at 4°C. Cells were subsequently washed and acquired through BD FACSCanto II and analyzed using FACSuite software (BD Biosciences). For gating synovial macrophages, peak of forward scatter width as singlet cells and forward scatter height to separate debris was selected. Cells were further stained by live/dead dye to obtain live cells and gated to identify double-positive $CD11b^{hi}$ and $CD64^{hi}$ synovial macrophages. Expression of indicated protein was further quantified from $CD11b^{hi}$ and $CD64^{hi}$ double-positive cells. In each experiment, a total of 100,000 events were collected. For transcript analysis, FACS-sorted $CD11b^{hi}$ and $CD64^{hi}$ double-positive synovial cells from indicated treatment groups of mice were collected and lysed in TRI reagent (T9424; Sigma-Aldrich) followed by cDNA synthesis to perform quantitative real-time PCR.

Immunofluorescence

For in vitro CHEMR23 visualization experiment, peritoneal macrophages from BALB/c mice were pretreated with ADA for 1 h followed by bacteria infection. Coverslips were incubated with primary CHEMR23 Ab overnight at 4°C, followed by 1-h incubation with DyLight 488–conjugated secondary Ab and nuclei staining with DAPI for 5 min. Coverslip was mounted on glycerol for confocal imaging. For in vivo tissue imaging, synovial tissue was resected and immediately preserved at −80°C. Cryosections of 5 μm were made in OCT medium and stained with primary Abs incubated overnight at 4°C. Sections were incubated with DyLight 488–conjugated secondary Ab for 1 h, and nuclei were stained with DAPI for 5 min. A coverslip was mounted on the section with glycerol as the medium. Confocal images were taken using a Zeiss LSM 710 Meta Confocal Laser Scanning Microscope, and images were analyzed using ZEN 2009 software.

Griess assay for nitrite estimation

Resected synovial tissue was digested in RPMI 1640 containing collagenase type IV (5 mg/ml) and DNase 1 (0.1 mg/ml) to obtain single-cell suspension. Cells were seeded at a density of 4 million per milliliter and incubated at 37°C and 5% CO_2. After 24 h, the culture supernatant was harvested to perform Griess assay. In a 96-well plate, 0.1 M stock solution of sodium nitrite was diluted to obtain a standard curve. A total of 50 μl of cell culture supernatant from each treatment group was mixed with an equal volume of Griess reagent, which consisted of 1% sulphanilamide solution with 5% H_3PO_4 and 0.1% *N*-1-napthylethylenediamine dihydrochloride solution. Samples were incubated for 20 min at room temperature in the dark, and absorbance was measured at 550 nm.

CFU assay

For in vitro CFU assay, peritoneal macrophages from BALB/c were infected with *S. aureus* at 10 MOI in DMEM for 4 h, followed by treatment with 200 μg/ml gentamicin for 2 h at 37°C. Cells were washed with PBS to kill extracellular bacteria, and macrophages were incubated further for indicated time points. To enumerate intracellular bacterial counts, macrophages were lysed in 0.05% SDS, and serial dilutions were plated on mannitol salt agar plates for positive selection of *S. aureus*. For in vivo CFU assay, hind limbs of BALB/c mice (which were intra-articularly infected with 1×10^7 CFU of live *S. aureus*) were dissected and crushed in tissue homogenizer (TissueLyser, 69982; QIAGEN) using 5-mm stainless steel beads (QIAGEN). Tissue lysate was serially diluted and plated on mannitol salt agar selection plates to obtain viable bacterial counts.

Statistical analysis

Levels of significance are expressed as mean ± SEM for the values from at least three or more independent experiments. GraphPad Prism 5.0 software was used for all the statistical analysis.

Results

Establishment of arthritis by S. aureus *infection*

For our current investigation, we have chosen *S. aureus* Cowan1 to study the development of septic arthritis. As reported, *S. aureus* Cowan1 is associated with arthritogenicity virulence factors, such as protein A (18, 19), fibrinogen-binding clumping factor A (ClfA) (20), and fibrinogen-binding proteins (FnBP) (21), that enhance the interaction with host cells and potentiate the tissue invasive ability by binding to collagen with high affinity. Interestingly, regardless of many reports, molecular pathways that govern host–*S. aureus* interactions and immune dysregulation require detailed investigation. In this context, we used a mouse model of septic arthritis, wherein intra-articular infection of *S. aureus* Cowan1 was administered in the left knee of BALB/c mice. The contralateral knee received PBS, which served as a control. Infected mice demonstrated symptoms of clinical arthritis 3 d postinfection, with observable limping and restricted leg movement. Seven days postinfection, the anterior knee and distal femur transverse cross-section (Fig. 1A) showed a visual increase in bone porosity as evaluated by micro–computed tomography. Quantification of bone morphometric indices indicated a decrease in bone volume percentage, trabecular thickness, and number with a simultaneous increase in trabecular space volume (Fig. 1B), collectively suggesting significant bone erosion upon infection.

In consonance with the described model, immunohistochemical analysis of knee sections obtained from *S. aureus*–infected mice displayed significant destruction of knee architecture along with recruitment of inflammatory cells within the joint space and into skeletal muscle bundles, indicating the extension of inflammation from the joint into the soft tissue of the limb (Fig. 1C). Scoring of synovial and bone erosion revealed a significant increase in synovial inflammation in addition to an increase in bone and cartilage damage (Fig. 1D). Interestingly, synovial fluid from arthritic patients is also reported to demonstrate altered cytokine profiles (22). For our current study, we have examined various chemokines that are known to regulate synovial inflammation and cartilage destruction. For example, CXCL1 and CCL2 have been shown to govern recruitment of neutrophils (23) and monocytes (24) in the synovium during arthritis. Furthermore, a study by Kuo et al. (25) has depicted genetic polymorphism in CCL4 and its association with increased susceptibility to rheumatoid arthritis. Other chemokines, such as CCL11 and CCL12, were assessed because of their direct effect on bone resorption and therapeutic targeting during arthritis progression (26, 27). In addition to this, our current investigation also explored the role of anti-inflammatory M2 macrophage in resolution of inflammation. Whereas both RETNLA and CX_3CR1 are known markers for resident synovial macrophages involved in restricting inflammation of joint tissues (28), UCP1 is known to regulate the reactive oxygen species to modulate inflammation (29). To elucidate mechanisms that regulate *S. aureus* infection–triggered inflammation, expression of a panel of inflammatory mediators was analyzed in the whole inflamed knee of mice. As indicated, expression profile of selected

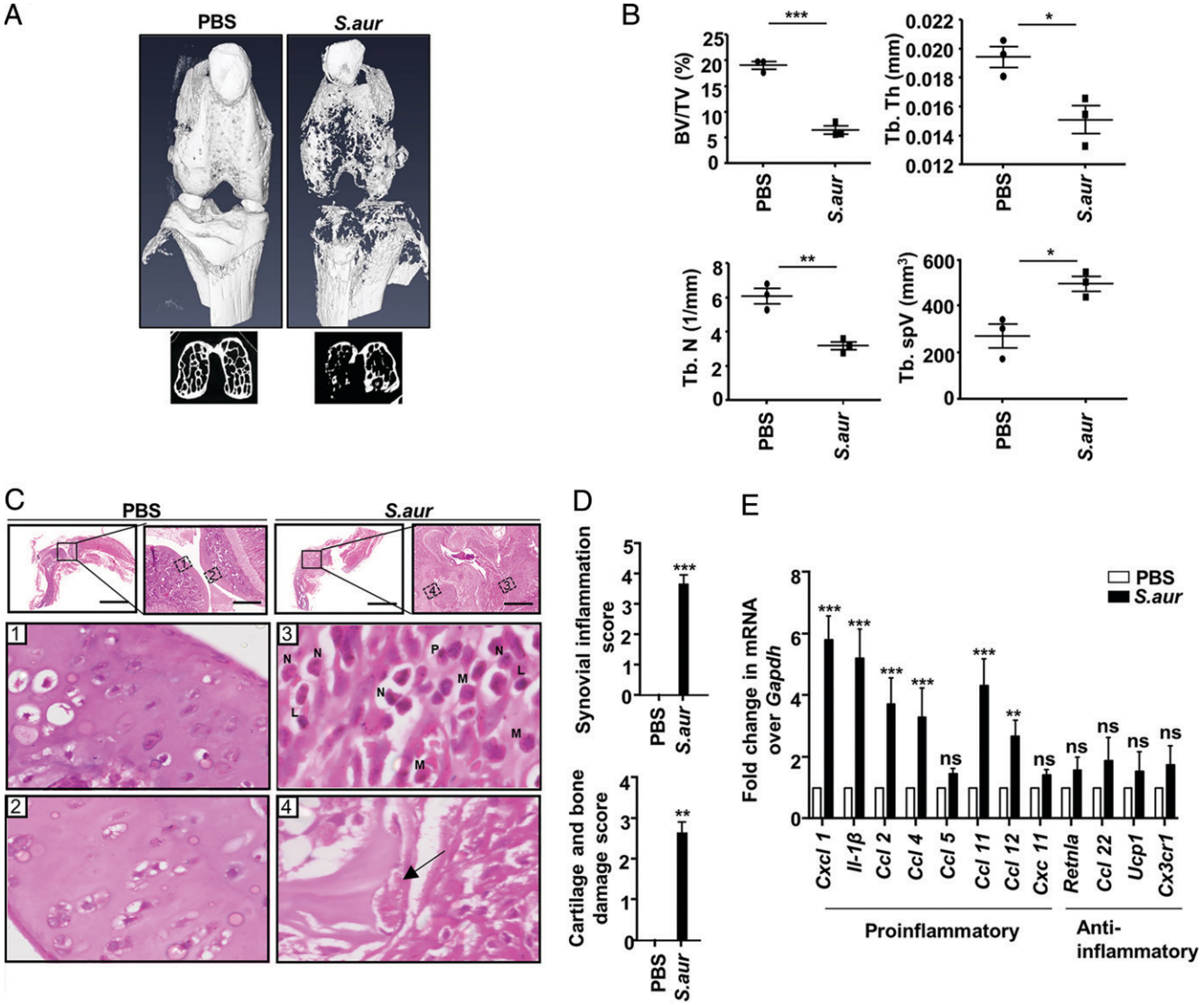

FIGURE 1. *S. aureus* Cowan1 is a causative agent of septic arthritis. (**A**–**E**) The left knee of BALB/c mice was intraarticularly injected with 10^7 CFU of live *S. aureus* on day 0. Contralateral knee received PBS. Mice were observed for 7 d, and subsequent experiments were performed. Representative micro-computed tomography images of day 7, showing (A) three-dimensional anterior knee and distal femur transverse cross-section of mice treated with PBS and infected with *S. aureus.* (B) Hind limbs were dissected for bone morphometric analysis utilizing different indices: bone volume/total volume (BV/TV, percentage), trabecular thickness (Tb. Th, millimeters), trabecular number (Tb .N, per millimeter), and trabecular space volume (Tb.spV, cubic millimeters) score. Symbols on scatter plot represent one mouse each. (C) Representative H&E-stained knee joints. Boxes 1 and 2 represent the intact articular cartilage and joint space. Box 3 represents the sheet of inflammatory cells within joint space. Box 4 represents damaged articular cartilage indicated by a black arrow. Scale bars, 1000 μm at low magnification and 200 μm at high magnification. Zoomed H&E-stained images of sections are at 100× magnification. (D) H&E-stained knee sections were scored for severity of synovial inflammation, cartilage, and bone damage. Each column represents pooled data from 3 mice. (E) On day 7, intraarticularly injected knees of BALB/c mice were pulverized, and quantitative real-time PCR analysis was performed for indicated molecules. Each column represents pooled data from six mice. Data represent the mean ± SEM of three independent experiments. $^*p < 0.05$, $^{**}p < 0.005$, $^{***}p < 0.001$, two-tailed unpaired Student *t* test. L, lymphocyte; M, macrophage; N, neutrophil; ns, not significant; P, plasma cell.

cytokines/chemokines demonstrated significant expression of proinflammatory cytokines as compared with anti-inflammatory cytokine signature (Fig. 1E). Consistent with this, the transcript profile of common inflammatory mediators also showed a similar increase of proinflammatory cytokine with no observable change in the levels of anti-inflammatory cytokines (Supplemental Fig. 1). Thus, these findings suggest that infection with *S. aureus* differentially regulated expression of proinflammatory mediators with increased bone porosity and bone erosion during the development of septic arthritis in mice.

ADA rescues S. aureus*–induced cartilage and bone damage*

Infection with *S. aureus* often leads to a drastic alteration of host tissue morphology endorsed with augmented expression of inflammatory cytokines. In this context, we sought to explore the preventive regimen to subside septic arthritis along with minimal adverse side effects. Therapeutic intervention with RA is shown to exhibit strong immunosuppressive effects against inflammatory diseases like colitis and allergic asthma (30, 31). Vitamin A deficiency is also reported to correlate with enhanced susceptibility to *S. aureus* infection (32). In this regard, ADA was administered daily to mice, starting from 3 d before giving *S. aureus* infection as a prophylactic treatment, and mice were kept under observation for 7 d (Fig. 2A). On day 7 postinfection, radiological examination of the anterior knee and distal femur transverse cross-section demonstrated that ADA treatment significantly reduced bone damage as observed through a

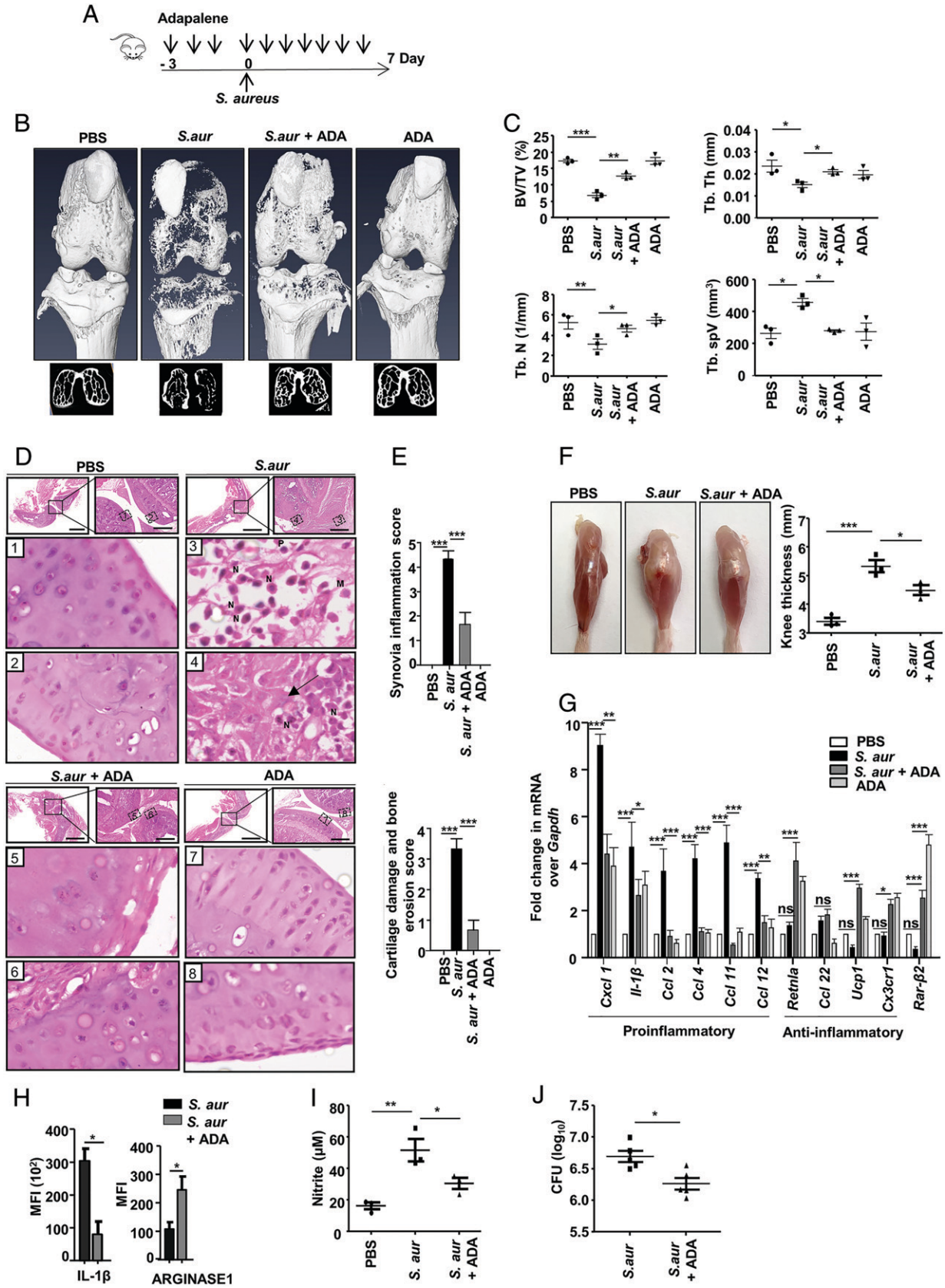

FIGURE 2. ADA negatively regulates *S. aureus*–induced septic arthritis. (**A**–**J**) Left knees of BALB/c mice were intra-articularly injected at day 0 with 10^7 CFU of live *S. aureus*. The contralateral knee received PBS. Mice were treated daily with ADA i.p. (5 mg/kg) starting at 3 d prior to bacterial infection and kept for 7 d. Representative micro–computed tomography images taken at 7 d of infection, showing (B) anterior knee and distal femur cross-section followed by (C) bone morphometric analysis using different indices: bone volume/total volume (BV/TV, percentage), trabecular thickness (Tb. Th, millimeters), trabecular number (Tb. N, per millimeter), and trabecular space volume (Tb.spV, cubic millimeter) score. Symbols on scatter plot *(Figure legend continues)*

decrease in bone porosity (Fig. 2B). Furthermore, bone morphometric measurement confirmed increased bone volume upon ADA treatment, with a significant increase in trabecular bone thickness and number along with a decreased volume of trabecular spaces (Fig. 2C). Histological analysis from knee sections upon treatment with ADA showed that recruitment of inflammatory cells is reduced with preserved articular cartilage and bone structure in *S. aureus*–infected mice (Fig. 2D). In this regard, double-blinded scoring demonstrated a significant decrease in synovial inflammation, bone, and cartilage damage of ADA-treated mice (Fig. 2E). Collectively, these data indicate that ADA treatment prevents *S. aureus*–induced irreversible tissue damage to the host.

Given the central role of inflammatory cytokines in septic arthritis pathogenesis, we explored if the observed rescue of tissue architecture upon ADA treatment correlates with modulation of cytokine profile and host bacterial burden. ADA treatment to *S. aureus*–infected mice demonstrated the reduction of knee edema (Fig. 2F). Transcript analysis from the whole knee joint upon treatment with ADA indicated a marked increase in expression of anti-inflammatory genes with a concomitant reduction in proinflammatory genes expression (Fig. 2G). *Rarβ2*, a known target for RA, was used as a positive control to assess in vivo activity of ADA. Similarly, we have also observed a skewed response toward anti-inflammatory cytokines with a significant increase in levels of *Tgf-β*, *Il-10*, and *Arg1* in the whole knee lysate (Supplemental Fig. 2). Moreover, the characterization of synovial macrophages revealed that ADA administration could significantly reduce expression of *S. aureus*–induced proinflammatory cytokine IL-1β, with a concomitant incr ease in anti-inflammatory ARGINASE1 expression (Fig. 2H, Supplemental Fig. 3A, 3B). We have further examined ADA-regulated inflammatory responses observed in Fig. 2G and Supplemental Fig. 2 in isolated synovial macrophages. We observed a significant reduction of proinflammatory markers, such as *Tnf-α, Cxcl1, Il-1β*, and *Nos2*, upon ADA treatment with a concomitant increase of anti-inflammatory genes like *Tgf-β, Il-10,* and *Arg1* (Supplemental Fig. 3C). The estimation of nitrite concentration also confirmed the anti-inflammatory effects of ADA (Fig. 2I). Further, in vivo CFU from hind limb indicated that ADA treatment of *S. aureus*–infected mice could significantly reduce the bacterial burden (Fig. 2J). However, we did not observe any significant change in bacterial count in vitro upon ADA treatment of peritoneal macrophages infected with *S. aureus* (Supplemental Fig. 4). Overall, these results suggest that ADA treatment primes host immune responses against *S. aureus* infection and prevents development of septic arthritis.

AURKA-responsive WNT signaling regulates S. aureus *infection–triggered septic arthritis*

To identify possible mechanisms driving the beneficial effects of ADA treatment, we focused on identification of signaling mediators that are cardinal to the pathogenesis of septic arthritis. Studies from our laboratory as well as from others have demonstrated a significant role for WNT signaling in the development of acute arthritis (16, 33). Importantly, WNT signaling is known to cross-talk with various signaling intermediates during immune dysregulation (34). Although activation of WNT signaling is known to entail increased inhibitory phosphorylation of GSK-3β with a concomitant decrease in pβ-CATENIN levels, signaling components orchestrating these events during septic arthritis have not been delineated. In this perspective, both AURKA and mTOR transcript levels are reported to be elevated in osteoclasts and B cells of patients with rheumatoid arthritis (35–37). To assess the role of AURKA as well as mTOR in regulating WNT signaling pathways, mice were infected with *S. aureus*, and infected knee sections were analyzed. As shown, the knee section of *S. aureus*–infected mice demonstrated activation of AURKA, which is marked by its phosphorylation at Threonine 288, along with activation of mTOR and WNT signaling axis (Fig. 3A). To explore the role of different pattern recognition receptors during septic arthritis, the involvement of TLR2, TLR4, and NOD2 was assessed. *S. aureus* infection to macrophages derived from TLR2 null mice or $tlr4^{Lps\text{-}d}$ showed no change in activation of AURKA, mTOR, and WNT signaling events compared with wild type, implicating that both TLR2 and TLR4 are dispensable for infection-induced activation of the said signaling pathway (data not shown). However, peritoneal macrophages that were subjected to RNA interference–mediated interference of NOD2 (also called caspase activating recruitment domain CARD15) diminished the ability of *S. aureus* to trigger activation of AURKA, mTOR, and WNT signaling (Fig. 3B), indicating a dominant role of NOD2 during *S. aureus*–mediated events.

To evaluate the interdependency of AURKA and mTOR in mediating activation of WNT signaling, macrophages were treated with alisertib (an AURKA-specific inhibitor) or rapamycin (mTOR-specific inhibitor), followed by infection with *S. aureus*. As observed. inhibition of AURKA activity downregulated the *S. aureus*–induced mTOR activity. However, rapamycin treatment could not inhibit infection-triggered AURKA activation (Fig. 3C), thereby indicating that mTOR is downstream to AURKA. To evaluate the functional relevance of AURKA activity, *S. aureus*–infected mice were administered alisertib daily after 3 d of the establishment of infection (Fig. 3D). Mice were sacrificed on day 7, and total protein was isolated from the hind limb to perform immunoblotting. As observed, the activation of the AURKA, mTOR, and WNT signaling axis was compromised upon alisertib treatment (Fig. 3E). Furthermore, the hind limb sections were evaluated by histopathology and scored for the severity of arthritis. Although the articular cartilage remained intact upon alisertib treatment, the presence of inflammatory cells was observed within the joint space, which focally involved periarticular soft tissue in both *S. aureus*–infected and alisertib-treated mice (Fig.

represent one mouse each. (D) Representative H&E-stained knee joints. Box 1 and 2 represent the intact articular cartilage and joint space. Box 3 indicates acute inflammation within joint space. Box 4 represents the extension of inflammatory cells into and destroying articular cartilage. Boxes 5 and 6 indicate intact articular cartilage with no sign of bone erosion. Boxes 7 and 8 showed the preserved articular cartage with no effect on tissue morphology due to ADA treatment alone. Scale bars, 1000 μm at low magnification and 200 μm at high magnification. Zoomed H&E-stained images of sections are at 100× magnification. (E) H&E sections were scored for severity of synovial inflammation, cartilage, and bone damage. Each column represents pooled data from three mice. (F) Representative images of knee edema and changes in the knee thickness measured by vernier caliper. Symbols on scatter plot represent one mouse each. (G) Knees were pulverized to perform quantitative real-time PCR for indicated target genes. Each column represents pooled data from six mice. (H) Mean fluoresce intensity of indicated molecule expression in synovial macrophages. Each column represents pooled data from synovial macrophages of 12 mice. (I) Synovial tissue supernatant from treated mice were cultured for 24 h followed by performing a Griess assay to estimate the nitrite concentration. Symbols on scatter plot represent one mouse each. (J) In vivo CFU of *S. aureus* from hind limbs of ADA-treated mice after 7 d of infection. Each value represents one hind limb, and five mice were used. Data represent the mean ± SEM of three independent experiments. $*p < 0.05$, $**p < 0.005$, $***p < 0.001$, one-way ANOVA followed by Tukey multiple comparisons test. M, macrophage; N, neutrophil; P, plasma cell.

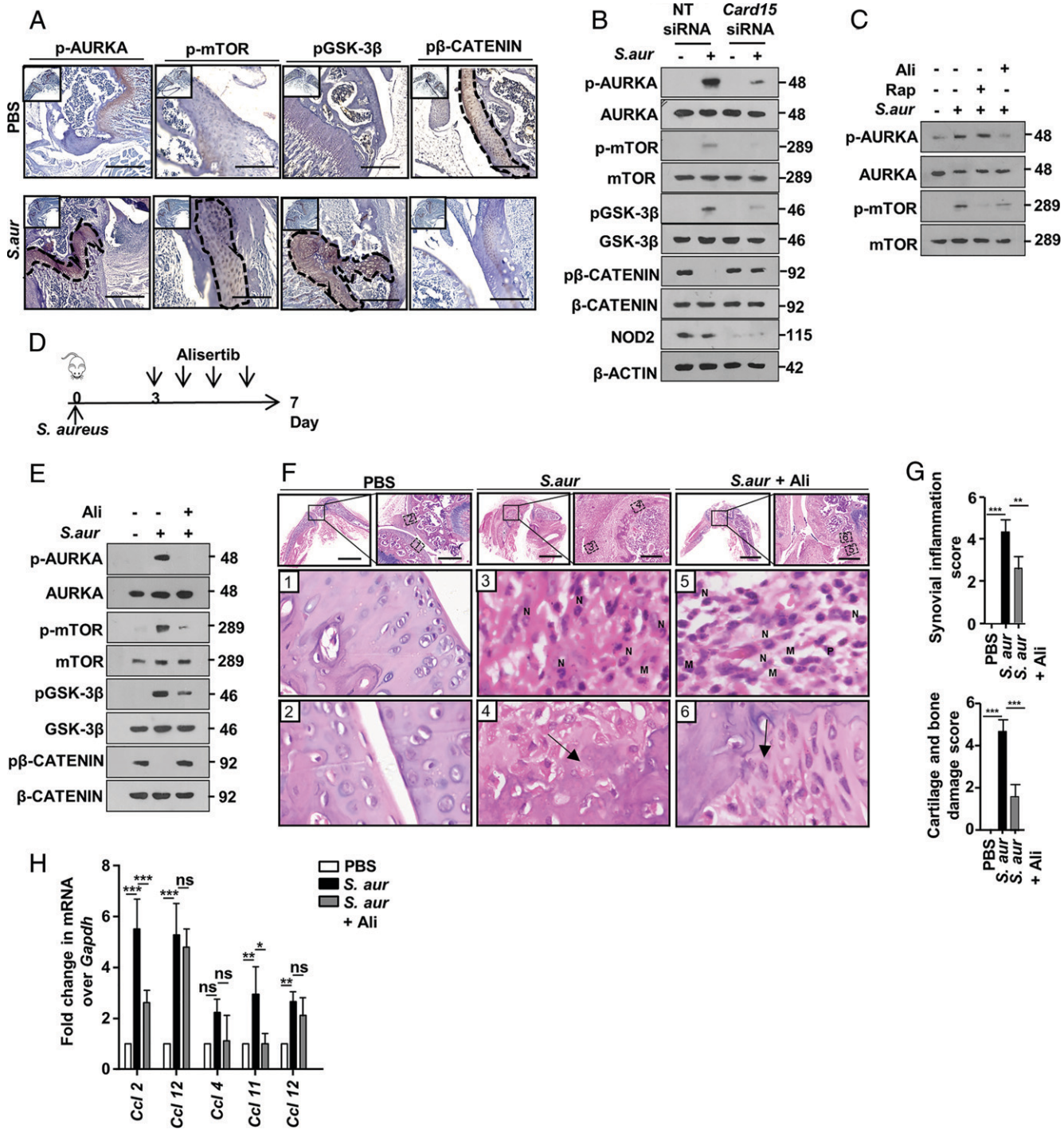

FIGURE 3. *S. aureus* induces NOD2-dependent activation of the AURKA–mTOR–WNT signaling axis. (**A**) The left knee of BALB/c mice was intra-articularly injected with 10^7 CFU of live *S. aureus* on day 0. The contralateral knee received PBS and was kept for 7 d. Representative images of immunohistochemistry that was performed on day 7 to check the activation of indicated molecules. Dotted line highlights the region of interest that stained positive for different proteins. Scale bar, 400 μm. (**B**) Peritoneal macrophages from BALB/c mice, transfected with nontargeting (NT) or *Card15* siRNA, were infected with *S. aureus* at MOI of 1:10 for 2 h. Immunoblotting was performed for indicated molecules. (**C**) Peritoneal macrophages from BALB/c mice were pretreated with alisertib and rapamycin for 1 h, followed by infection with *S. aureus* at MOI 1:10 for 2 h, and immunoblotting was performed for indicated molecules. (**D**–**H**) After 3 d of *S. aureus* infection, mice were treated daily with alisertib i.p. (3 mg/kg). After 7 d, knees (E) were pulverized to perform immunoblotting for indicated proteins. (F) Knees were sectioned and stained with H&E. Boxes 1 and 2 represent the intact articular cartilage and joint space. Boxes 3 and 5 indicate myeloid cells present within the joint space and extending into the surface of the articular cartilage. Boxes 4 and 6 represent damaged articular cartilage (black arrow). Bar, 1000 μm at low magnification and 200 μm at high magnification. Zoomed H&E-stained images of sections are at 100× magnification. (G) H&E sections were scored for severity of synovial inflammation, cartilage, and bone damage. Each column represents pooled data from three mice. (H) Knees were also pulverized to perform quantitative real-time PCR for indicated target genes. Each column represents pooled data from six mice. Sequential 5-μm-thick sections were used for immunostaining. Data represent the mean ± SEM of three independent experiments. Blots are representative of three independent experiments. $^{**}p < 0.005$, $^{***}p < 0.001$, one-way ANOVA followed by Tukey multiple-comparisons test. M, macrophage; N, neutrophil.

3F). Upon scoring of knee sections, it was found that alisertib treatment could reduce synovial inflammation as well as decrease cartilage and bone destruction (Fig. 3G), albeit in a lesser manner than ADA treatment (Fig. 2E). Transcript analysis revealed that expression of only a few selective proinflammatory cytokines was reduced (Fig. 3H), suggesting that alisertib treatment could partially rescue the inflammation. Collectively, our findings suggest that AURKA signaling contributes significantly to septic arthritis development.

ADA differentially regulates S. aureus*–induced WNT and HIPPO signaling*

Next, the treatment of ADA was used to monitor its effects on the AURKA signaling axis. Immunoblotting of knee samples showed that ADA treatment impedes *S. aureus*–induced AURKA–WNT signaling axis (Fig. 4A). However, previous experiments indicated that the targeted inhibition of AURKA activity could only partially limit inflammation (Fig. 3G, 3H). This led us to hypothesize the possible involvement of an additional signaling cascade that coordinates the therapeutic effects of ADA treatment and controls inflammation. RARγ, a nuclear receptor, is known to regulate Hippo-Yap signaling in tumorigenesis and metastasis of colorectal cancer (38). MST1/2 kinases are key mediators of HIPPO signaling. Studies using MST1/2 knockout mice have reported enhanced susceptibility to bacterial sepsis (39) and also greatly impaired endochondral ossification, which is required during fracture healing and bone repair (40). With this premise, the activation of HIPPO signaling was assessed. Phosphorylation of MST1/2 and LATS1/2 is indicative of Hippo signaling activation. Immunoblotting assay of infected knee samples of mice showed that *S. aureus* infection induced the activatory phosphorylation of MST1, MST2, and LATS1, which was further augmented upon ADA treatment, in contrast to the strong suppressive effect of ADA on the *S. aureus*–induced WNT signaling pathway, as shown by inhibition of GSK-3β with concomitant activation of pβ-CATENIN (Fig. 4B). Similarly, immunofluorescence staining of synovial tissue of mice treated with ADA upon infection with *S. aureus* validated our observations of enhancement of HIPPO signaling with concomitant inhibition of the WNT signaling pathway (Fig. 4C). To elucidate the signaling intermediates between ADA and the HIPPO pathway, a screen for specific signaling events previously documented to be activated by RA was performed. Macrophages

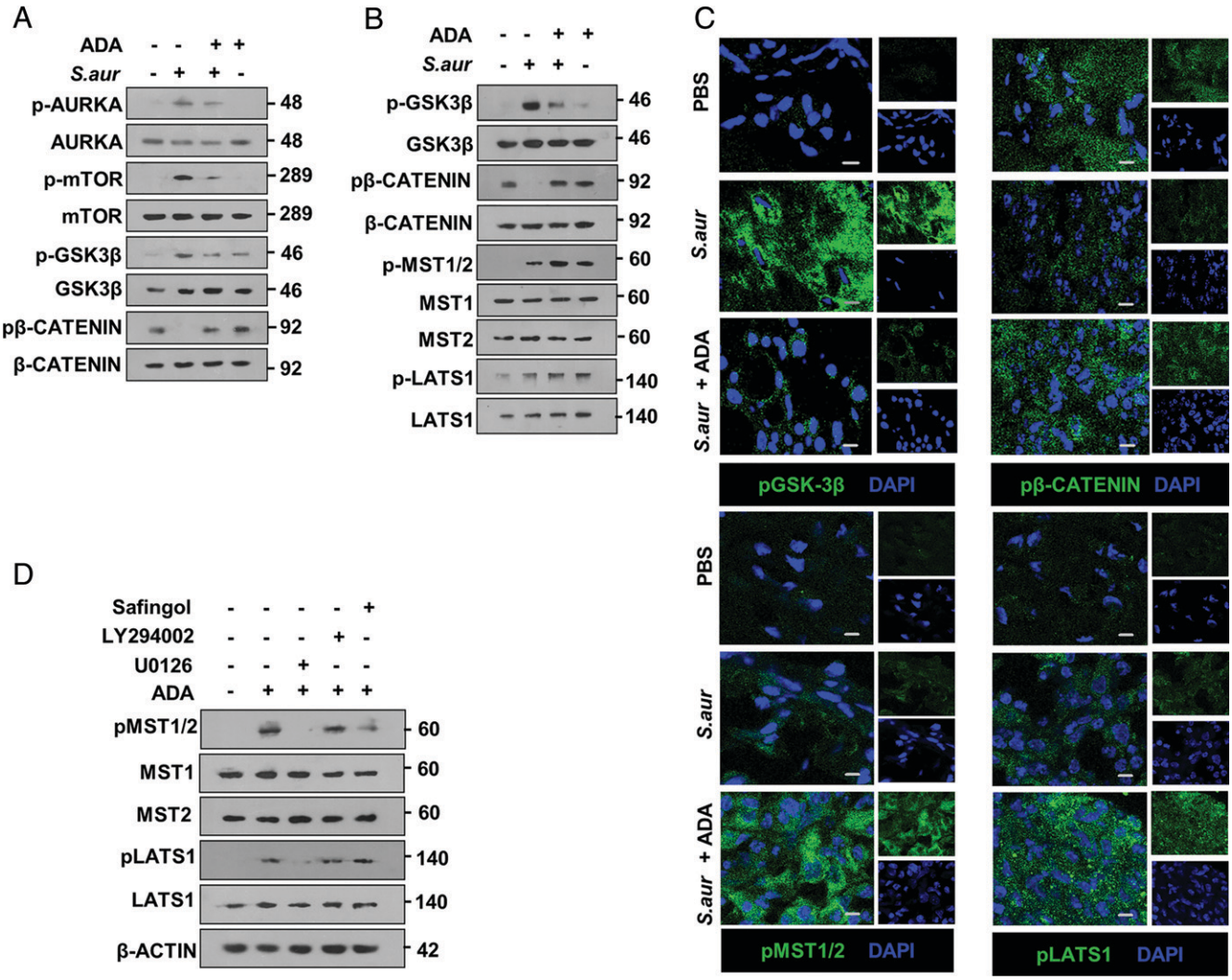

FIGURE 4. ADA treatment inhibits WNT and activates HIPPO signaling. (**A**–**C**) Left knees of BALB/c mice were intra-articularly injected at day 0 with 10^7 CFU of *S. aureus*. Contralateral knee received PBS. Mice were treated daily with ADA i.p. (5 mg/kg) starting at 3 d prior to bacterial infection and kept for 7 d. Representative (A and B) immunoblotting of pulverized knee samples and (C) immunofluorescence from knee synovium cryosections were performed to assess activation of WNT and HIPPO signaling. Scale bar, 5 μm with original magnification 40×. (**D**) Peritoneal macrophages from BALB/c mice were treated with indicated inhibitors for 1 h followed by treatment with ADA (5 μM) for 1 h. Immunoblotting was performed to assess activation of HIPPO signaling. Data are representative of three independent experiments.

were treated with specific inhibitors of MAPK/ERK (U0126), PI3K (LY294002), and pan PKC (Safingol), of which U0126 showed significant abrogation of ADA-induced phosphorylation of MST1/2 and LATS1 (Fig. 4D). Thus, ADA-triggered activation of HIPPO signaling requires participation of MAPK/ERK.

HIPPO signaling regulates inflammation

To further delineate the regulatory role of ADA-induced HIPPO signaling, peritoneal macrophages were subjected to siRNA-mediated silencing of MST1/2 (also known as serine threonine kinase STK3/4). Inhibition of HIPPO signaling did not significantly alter expression levels of a panel of proinflammatory cytokines, except the marginal effect found on transcript levels of *Ccl2*. Interestingly, it showed a significant reduction of ADA-induced anti-inflammatory transcripts (Fig. 5A). These observations implicate the modulatory role of ADA-driven Hippo signaling in mediating macrophage polarization toward an anti-inflammatory state.

Lipid-derived class of proresolvin mediators are shown to subside host-driven hyperinflammation with reduced collateral tissue damage and amplified bacterial clearance (41, 42). Given the implicit role of HIPPO signaling in regulating the inflammatory state of macrophages, we sought to explore the effects of HIPPO on resolvins, as well. CHEMR23, a G protein–coupled receptor, is known to resolve acute as well as chronic inflammation in presence of its ligand Resolvin-E1 (RvE1) (43–45). As shown, a significant increase in cell membrane localization of CHEMR23 was observed upon ADA treatment compared with *S. aureus* infection alone (Fig. 5B), and silencing of MST1/2 resulted in the abrogation of CHEMR23 protein expression (Fig. 5C). These results are indicative of the plausible role of CHEMR23 in subduing inflammation, which could have been driven by HIPPO signaling upon treatment of ADA. However, further studies are required to understand the role of resolvins against septic arthritis development. In summary, we have found that *S. aureus* infection triggers robust infiltration of inflammatory chemokines in the knee synovium that is associated with cartilage and bone damage. At a molecular level, *S. aureus* activates AURKA-regulated WNT signaling, which showed a pivotal role in septic arthritis development. Furthermore, for our current model, we have employed ADA prophylaxis and found its beneficial effects in preventing the tissue damage and host bacterial burden. Mechanistically, ADA governed the activation of MST1/2, which regulated expression of anti-inflammatory M2 and resolvins, thereby establishing the repressive role of ADA in *S. aureus*–induced septic arthritis.

Discussion

Septic arthritis pathogenesis often involves hyperinflammation that renders permanent damage to the infected surrounding soft tissue and may spread to bones, as well (46, 47). The hyperinflammation results in prolonged induction of Th1 or M1 macrophage cytokines, which contributes to said pathogenesis, and often, cotreatment of antibiotics and immunosuppressive steroids are advised as a cure to septic arthritis patients. However, the relative risk associated with steroids therapy predisposes patients to severe contraindications, including osteoporosis (48) along with diabetes mellitus and adrenal insufficiency (49). Also, extensive use of antibiotics resulted in the emergence of methicillin (β-lactam antibiotic) resistance with increased risk of mortality among septic arthritis patients (50).

Our finding that NOD2 is critical for septic arthritis development is consistent with the previously published literature that showed innate sensing of *S. aureus* by NOD2 is required for elicitation of host immune responses (51, 52). The current study highlights the important role of AURKA activation in septic arthritis development. However, administration of alisertib, AURKA inhibitor, only marginally prevented *S. aureus*–induced inflammatory response. Moreover, alisertib is not a certified FDA therapeutic as it failed in phase III clinical trial (53). In view of such reports, we used FDA-approved drug ADA in curtailing *S. aureus*–triggered septic arthritis. ADA treatment was found to differentially regulate inhibition of *S. aureus*–triggered WNT signaling with concomitant activation of the HIPPO pathway. Furthermore, ADA-driven HIPPO pathway activation potentiated the anti-inflammatory response of synovial macrophages, leading to suppressed joint inflammation. We also observed that ADA treatment significantly reduced the *S. aureus* burden in vivo; however, no change was observed in in vitro bacterial count. We would like to emphasize in this article that in vitro studies solely cannot predict the effects of a drug on the susceptibility of a pathogen. This may be due to complex and heterogenous systemic conditions that prevail in a host that impart challenges to pathogen survival (54). Moreover, treatment with RA is known to exert pleiotropic effects by targeting different responsive cells, including T cells, B cells, dendritic cells, fibroblasts, and so on, which may dictate systemic responses of the host to RA therapy (55). Specifically, RA-modulated differentiation of naive T cells into Treg cell can govern the inflammation (30). Moreover, RA is also reported to regulate T cell activation and favors Th1/Th2 balance toward Th2 phenotype (56–58). Although macrophages seem to mediate the anti-inflammatory properties of ADA in septic arthritis, the indirect role of T cell subsets, such as Tregs and Th2, in establishing anti-inflammatory phenotype of macrophages and promotion of tissue repair cannot be ruled out.

In our study, we propose ADA as potential drug therapy to prevent septic arthritis. Mechanistically, ADA was found to potentiate HIPPO signaling–mediated anti-inflammatory response. siRNA-mediated silencing of HIPPO further entrenched our observation as we found attenuated anti-inflammatory response with a decrease in levels of M2 macrophage markers and resolvins. Therefore, the observed in vivo effect of the ADA drug was found to be quite specific and circuits through positive regulation of HIPPO signaling. However, we cannot rule out the possibility that inhibitory drugs can cross-regulate through different signaling mediators. ADA is known to regulate cyclin-dependent kinases involved in cell cycle arrest and induction of apoptosis, which has not been explored in the current study (59, 60). The use of other pharmacological inhibitors like alisertib may also cross-talk with the PI3K/AKT pathway to govern the pathogenesis of rheumatoid arthritis (61). Overall, although our current study focuses on WNT and HIPPO pathways, it is still important to explore in vivo combinatorial effects of drug treatment through future studies. Furthermore, in the case of host–microbial interactions, resolution of ensuing inflammation often involves recruitment of lipid-derived mediators such as resolvins to the local inflammatory milieu. In this study, we have demonstrated that HIPPO signaling potentiated by ADA regulated the level of membrane-bound CHEMR23 in macrophages. However, direct effects of RvE1 treatment are not explored in the current work.

In summary, to our knowledge, we elucidate a novel mechanism of AURKA–WNT signaling that regulates *S. aureus*–mediated septic arthritis development. Furthermore, ADA was found to dictate functional cross-talk between WNT and the HIPPO pathway, thereby mounting anti-inflammatory macrophage polarization and possible recruitment of resolvins in knee joints of mice. Thus, we propose that ADA could act as a promising candidate to treat septic arthritis. Finally, given the importance of differential modulation of the WNT and HIPPO signaling axis, future studies would benefit from exploration of the relative contribution of different signaling

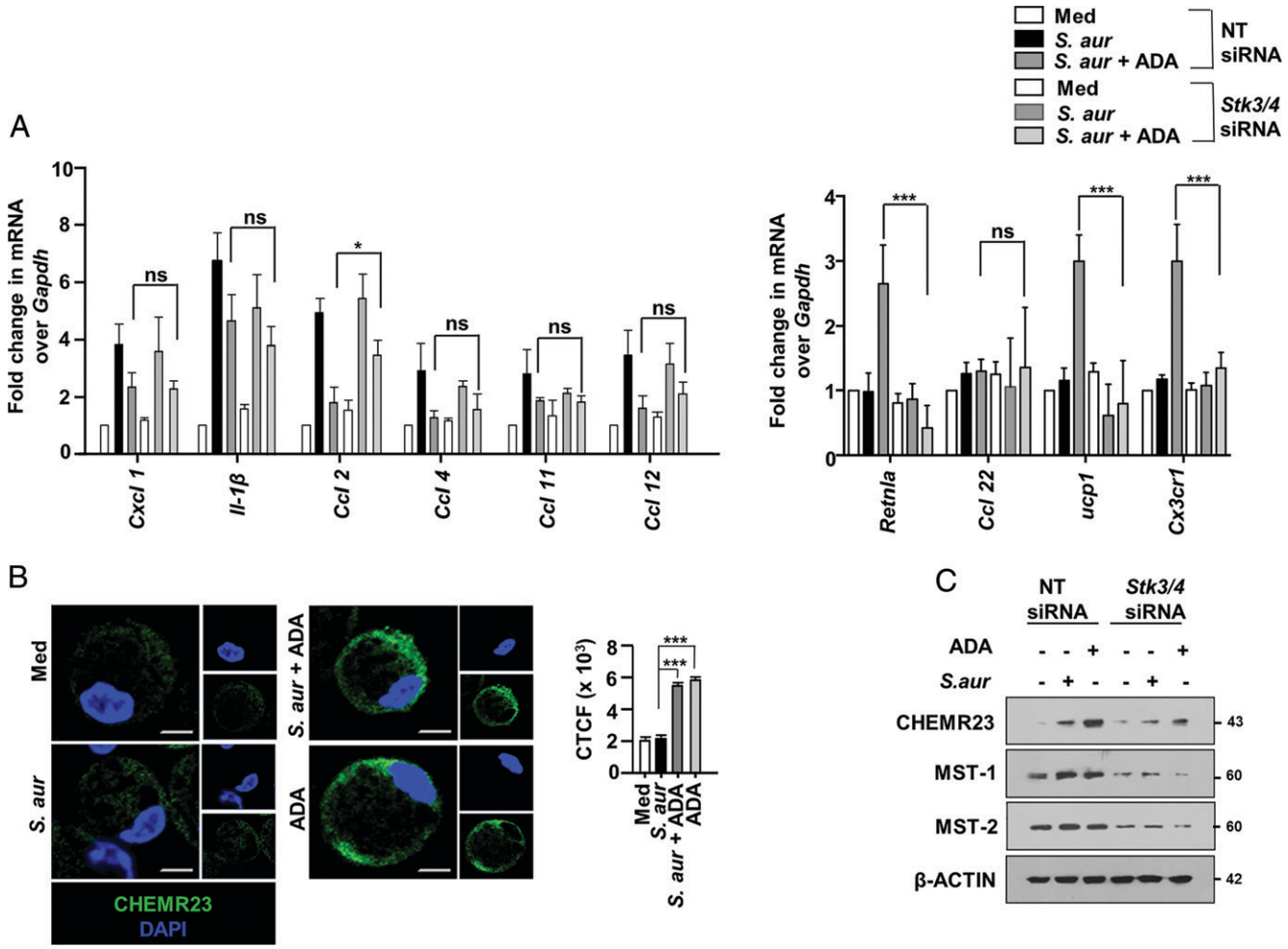

FIGURE 5. ADA-induced HIPPO signaling regulates anti-inflammatory macrophages and CHEMR23 expression. (**A**) Peritoneal macrophages from BALB/c mice transfected with nontargeting (NT) or *STK3/4* siRNA were treated with ADA for 2 h, followed by infection with *S. aureus* for 12 h. Quantitative real-time PCR was performed to analyze transcript level of indicated genes. (**B**) Peritoneal macrophages from BALB/c mice were treated with ADA for 2 h, followed by infection with *S. aureus* for 12 h. Representative immunofluorescence images of CHEMR23 receptor localization. Based on immunofluorescence images, corrected total cell fluorescence (CTCF) was calculated ($n = 100$, each treatment) and plotted. Scale bar, 5 μm with original magnification ×63. (**C**) Peritoneal macrophages from BALB/c mice transfected with NT or *STK3/4* siRNA were treated with ADA for 2 h, followed by infection with *S. aureus* for 12 h. Immunoblotting was performed to check CHEMR23 protein level. Data represent the mean ± SEM of three independent experiments. $*p < 0.05$, $***p < 0.001$, one-way ANOVA followed by Tukey multiple comparisons. ns, not significant.

pathways during septic arthritis pathogenesis. Also, several aspects of the current study, including the effects of distinct cell type present in the inflammatory milieu along with the role of bioactive mediators and possible use of ADA as an adjunct therapy with antibiotics, can pose relevance and new avenues for future studies.

Acknowledgments

We thank the Central Animal Facility, Indian Institute of Science, for providing mice and acknowledge Dr. Subbaraya G. Ramachandra for guidance. We thank Dr. Madhavi Naik, consulting pathologist, St. Theresa Hospital, Bangalore, for blinded histopathological analysis. We are also grateful to the Department of Microbiology and Cell Biology confocal facility, the flow cytometry facility, and the Advanced Facility for Microscopy and Microanalysis, Indian Institute of Science. We thank Dr. Ravi Manjithaya for providing access to the slide scanner microscopy facility at the Jawaharlal Nehru Centre for Advanced Scientific Research (JNCASR), Bangalore. We thank Dr. Kushagra Bansal, JNCASR, for suggestions and valuable inputs. We are thankful to Dr. Rachit Agarwal and Ameya Dravid for help with tissue homogenization. K.N.B. laboratory members Gaurav Lohia, Awantika Shah, Mahima, and Ankita Ghoshal are acknowledged for help.

Disclosures

The authors have no financial conflicts of interest.

References

1. Frazee, B. W., C. Fee, and L. Lambert. 2009. How common is MRSA in adult septic arthritis? *Ann. Emerg. Med.* 54: 695–700.
2. Lin, W.-T., C.-D. Wu, S.-C. Cheng, C.-C. Chiu, C.-C. Tseng, H.-T. Chan, P.-Y. Chen, and C.-M. Chao. 2015. High prevalence of methicillin-resistant *Staphylococcus aureus* among patients with septic arthritis caused by *Staphylococcus aureus*. *PLoS One* 10: e0127150.
3. Fowler, V. G., Jr., J. M. Miro, B. Hoen, C. H. Cabell, E. Abrutyn, E. Rubinstein, G. R. Corey, D. Spelman, S. F. Bradley, B. Barsic, et al. 2005. *Staphylococcus aureus* endocarditis: a consequence of medical progress. *JAMA* 293: 3012–3021.
4. Cosgrove, S. E., G. Sakoulas, E. N. Perencevich, M. J. Schwaber, A. W. Karchmer, and Y. Carmeli. 2003. Comparison of mortality associated with methicillin-resistant and methicillin-susceptible *Staphylococcus aureus* bacteremia: a meta-analysis. *Clin. Infect. Dis.* 36: 53–59.
5. Kavanagh, N., E. J. Ryan, A. Widaa, G. Sexton, J. Fennell, S. O'Rourke, K. C. Cahill, C. J. Kearney, F. J. O'Brien, and S. W. Kerrigan. 2018. Staphylococcal osteomyelitis: disease progression, treatment challenges, and future directions. *Clin. Microbiol. Rev.* 31: e00084-17.
6. Edwards, C. J., C. Cooper, D. Fisher, M. Field, T. P. van Staa, and N. K. Arden. 2007. The importance of the disease process and disease-modifying antirheumatic drug treatment in the development of septic arthritis in patients with rheumatoid arthritis. *Arthritis Rheum.* 57: 1151–1157.

7. Galloway, J. B., K. L. Hyrich, L. K. Mercer, W. G. Dixon, A. P. Ustianowski, M. Helbert, K. D. Watson, M. Lunt, D. P. M. Symmons, and BSR Biologics Register. 2011. Risk of septic arthritis in patients with rheumatoid arthritis and the effect of anti-TNF therapy: results from the British Society for Rheumatology Biologics Register. *Ann. Rheum. Dis.* 70: 1810–1814.
8. Elias, K. M., A. Laurence, T. S. Davidson, G. Stephens, Y. Kanno, E. M. Shevach, and J. J. O'Shea. 2008. Retinoic acid inhibits Th17 polarization and enhances FoxP3 expression through a Stat-3/Stat-5 independent signaling pathway. *Blood* 111: 1013–1020.
9. Manicassamy, S., R. Ravindran, J. Deng, H. Oluoch, T. L. Denning, S. P. Kasturi, K. M. Rosenthal, B. D. Evavold, and B. Pulendran. 2009. Toll-like receptor 2-dependent induction of vitamin A-metabolizing enzymes in dendritic cells promotes T regulatory responses and inhibits autoimmunity. *Nat. Med.* 15: 401–409.
10. Nozaki, Y., T. Yamagata, M. Sugiyama, S. Ikoma, K. Kinoshita, and M. Funauchi. 2006. Anti-inflammatory effect of all-trans-retinoic acid in inflammatory arthritis. *Clin. Immunol.* 119: 272–279.
11. Czernielewski, J., S. Michel, M. Bouclier, M. Baker, and J. C. Hensby. 2001. Adapalene biochemistry and the evolution of a new topical retinoid for treatment of acne. *J. Eur. Acad. Dermatol. Venereol.* 15(Suppl 3): 5–12.
12. Rioja, I., K. A. Bush, J. B. Buckton, M. C. Dickson, and P. F. Life. 2004. Joint cytokine quantification in two rodent arthritis models: kinetics of expression, correlation of mRNA and protein levels and response to prednisolone treatment. *Clin. Exp. Immunol.* 137: 65–73.
13. Sheibanie, A. F., T. Khayrullina, F. F. Safadi, and D. Ganea. 2007. Prostaglandin E2 exacerbates collagen-induced arthritis in mice through the inflammatory interleukin-23/interleukin-17 axis. *Arthritis Rheum.* 56: 2608–2619.
14. Bouxsein, M. L., S. K. Boyd, B. A. Christiansen, R. E. Guldberg, K. J. Jepsen, and R. Müller. 2010. Guidelines for assessment of bone microstructure in rodents using micro-computed tomography. *J. Bone Miner. Res.* 25: 1468–1486.
15. Hsieh, W. S., C. C. Kung, S. L. Huang, S. C. Lin, and W. H. Sun. 2017. TDAG8, TRPV1, and ASIC3 involved in establishing hyperalgesic priming in experimental rheumatoid arthritis. *Sci. Rep.* 7: 8870.
16. Singh, V., S. Holla, S. G. Ramachandra, and K. N. Balaji. 2015. WNT-inflammasome signaling mediates NOD2-induced development of acute arthritis in mice. *J. Immunol.* 194: 3351–3360.
17. Futami, I., M. Ishijima, H. Kaneko, K. Tsuji, N. Ichikawa-Tomikawa, R. Sadatsuki, T. Muneta, E. Arikawa-Hirasawa, I. Sekiya, and K. Kaneko. 2012. Isolation and characterization of multipotential mesenchymal cells from the mouse synovium. *PLoS One* 7: e45517.
18. Palmqvist, N., T. Foster, A. Tarkowski, and E. Josefsson. 2002. Protein A is a virulence factor in *Staphylococcus aureus* arthritis and septic death. *Microb. Pathog.* 33: 239–249.
19. Kronvall, G., J. H. Dossett, P. G. Quie, and R. C. Williams. 1971. Occurrence of protein a in staphylococcal strains: quantitative aspects and correlation to antigenic and bacteriophage types. *Infect. Immun.* 3: 10–15.
20. Palmqvist, N., T. Foster, J. R. Fitzgerald, E. Josefsson, and A. Tarkowski. 2005. Fibronectin-binding proteins and fibrinogen-binding clumping factors play distinct roles in staphylococcal arthritis and systemic inflammation. *J. Infect. Dis.* 191: 791–798.
21. Sinha, B., P. Francois, Y. A. Que, M. Hussain, C. Heilmann, P. Moreillon, D. Lew, K. H. Krause, G. Peters, and M. Herrmann. 2000. Heterologously expressed *Staphylococcus aureus* fibronectin-binding proteins are sufficient for invasion of host cells. *Infect. Immun.* 68: 6871–6878.
22. McInnes, I. B., and G. Schett. 2007. Cytokines in the pathogenesis of rheumatoid arthritis. *Nat. Rev. Immunol.* 7: 429–442.
23. Coelho, F. M., V. Pinho, F. A. Amaral, D. Sachs, V. V. Costa, D. H. Rodrigues, A. T. Vieira, T. A. Silva, D. G. Souza, R. Bertini, et al. 2008. The chemokine receptors CXCR1/CXCR2 modulate antigen-induced arthritis by regulating adhesion of neutrophils to the synovial microvasculature. *Arthritis Rheum.* 58: 2329–2337.
24. Raghu, H., C. M. Lepus, Q. Wang, H. H. Wong, N. Lingampalli, F. Oliviero, L. Punzi, N. J. Giori, S. B. Goodman, C. R. Chu, et al. 2017. CCL2/CCR2, but not CCL5/CCR5, mediates monocyte recruitment, inflammation and cartilage destruction in osteoarthritis. *Ann. Rheum. Dis.* 76: 914–922.
25. Kuo, S. J., C. C. Huang, C. H. Tsai, H. C. Hsu, C. M. Su, and C. H. Tang. 2018. Chemokine C-C motif ligand 4 gene polymorphisms associated with susceptibility to rheumatoid arthritis. *BioMed Res. Int.* 2018: 9181647.
26. Kindstedt, E., C. K. Holm, R. Sulniute, I. Martinez-Carrasco, R. Lundmark, and P. Lundberg. 2017. CCL11, a novel mediator of inflammatory bone resorption. *Sci. Rep.* 7: 5334.
27. Quinones, M. P., C. A. Estrada, Y. Kalkonde, S. K. Ahuja, W. A. Kuziel, M. Mack, and S. S. Ahuja. 2005. The complex role of the chemokine receptor CCR2 in collagen-induced arthritis: implications for therapeutic targeting of CCR2 in rheumatoid arthritis. *J. Mol. Med. (Berl.)* 83: 672–681.
28. Culemann, S., A. Grüneboom, J. Á. Nicolás-Ávila, D. Weidner, K. F. Lämmle, T. Rothe, J. A. Quintana, P. Kirchner, B. Krljanac, M. Eberhardt, et al. 2019. Locally renewing resident synovial macrophages provide a protective barrier for the joint. *Nature* 572: 670–675.
29. Urban, H., and C. B. Little. 2018. The role of fat and inflammation in the pathogenesis and management of osteoarthritis. *Rheumatology (Oxford)* 57(suppl_4): iv10–iv21.
30. Mucida, D., Y. Park, G. Kim, O. Turovskaya, I. Scott, M. Kronenberg, and H. Cheroutre. 2007. Reciprocal TH17 and regulatory T cell differentiation mediated by retinoic acid. *Science* 317: 256–260.
31. Goswami, S., P. Angkasekwinai, M. Shan, K. J. Greenlee, W. T. Barranco, S. Polikepahad, A. Seryshev, L. Z. Song, D. Redding, B. Singh, et al. 2009. Divergent functions for airway epithelial matrix metalloproteinase 7 and retinoic acid in experimental asthma. *Nat. Immunol.* 10: 496–503.
32. Wiedermann, U., A. Tarkowski, T. Bremell, L. Å. Hanson, H. Kahu, and U. I. Dahlgren. 1996. Vitamin A deficiency predisposes to *Staphylococcus aureus* infection. *Infect. Immun.* 64: 209–214.
33. Saha, S., J. Qi, S. Wang, M. Wang, X. Li, Y. G. Kim, G. Núñez, D. Gupta, and R. Dziarski. 2009. PGLYRP-2 and Nod2 are both required for peptidoglycan-induced arthritis and local inflammation. *Cell Host Microbe* 5: 137–150.
34. Mukherjee, T., V. A. V. Udupa, P. Prakhar, K. Chandra, D. Chakravortty, and K. N. Balaji. 2019. Epidermal growth factor receptor-responsive indoleamine 2,3-dioxygenase confers immune homeostasis during *Shigella flexneri* infection. *J. Infect. Dis.* 219: 1841–1851.
35. Cejka, D., S. Hayer, B. Niederreiter, W. Sieghart, T. Fuereder, J. Zwerina, and G. Schett. 2010. Mammalian target of rapamycin signaling is crucial for joint destruction in experimental arthritis and is activated in osteoclasts from patients with rheumatoid arthritis. *Arthritis Rheum.* 62: 2294–2302.
36. Glant, T. T., T. Besenyei, A. Kádár, J. Kurkó, B. Tryniszewska, J. Gál, G. Soós, Z. Szekanecz, G. Hoffmann, J. A. Block, et al. 2013. Differentially expressed epigenome modifiers, including aurora kinases A and B, in immune cells in rheumatoid arthritis in humans and mouse models. *Arthritis Rheum.* 65: 1725–1735.
37. Laragione, T., and P. S. Gulko. 2010. mTOR regulates the invasive properties of synovial fibroblasts in rheumatoid arthritis. *Mol. Med.* 16: 352–358.
38. Guo, P. D., X. X. Lu, W. J. Gan, X. M. Li, X. S. He, S. Zhang, Q. H. Ji, F. Zhou, Y. Cao, J. R. Wang, et al. 2016. RARγ downregulation contributes to colorectal tumorigenesis and metastasis by derepressing the hippo-yap pathway. *Cancer Res.* 76: 3813–3825.
39. Geng, J., X. Sun, P. Wang, S. Zhang, X. Wang, H. Wu, L. Hong, C. Xie, X. Li, H. Zhao, et al. 2015. Kinases Mst1 and Mst2 positively regulate phagocytic induction of reactive oxygen species and bactericidal activity. *Nat. Immunol.* 16: 1142–1152.
40. Deng, Y., A. Wu, P. Li, G. Li, L. Qin, H. Song, and K. K. Mak. 2016. Yap1 regulates multiple steps of chondrocyte differentiation during skeletal development and bone repair. *Cell Rep.* 14: 2224–2237.
41. Abdulnour, R. E., H. P. Sham, D. N. Douda, R. A. Colas, J. Dalli, Y. Bai, X. Ai, C. N. Serhan, and B. D. Levy. 2016. Aspirin-triggered resolvin D1 is produced during self-resolving gram-negative bacterial pneumonia and regulates host immune responses for the resolution of lung inflammation. *Mucosal Immunol.* 9: 1278–1287.
42. Serhan, C. N., and B. D. Levy. 2018. Resolvins in inflammation: emergence of the pro-resolving superfamily of mediators. *J. Clin. Invest.* 128: 2657–2669.
43. Herová, M., M. Schmid, C. Gemperle, and M. Hersberger. 2015. ChemR23, the receptor for chemerin and resolvin E1, is expressed and functional on M1 but not on M2 macrophages. *J. Immunol.* 194: 2330–2337.
44. Schwab, J. M., N. Chiang, M. Arita, and C. N. Serhan. 2007. Resolvin E1 and protectin D1 activate inflammation-resolution programmes. *Nature* 447: 869–874.
45. Arita, M., T. Ohira, Y.-P. Sun, S. Elangovan, N. Chiang, and C. N. Serhan. 2007. Resolvin E1 selectively interacts with leukotriene B4 receptor BLT1 and ChemR23 to regulate inflammation. *J. Immunol.* 178: 3912–3917.
46. Corrado, A., P. Donato, S. Maccari, R. Cecchi, T. Spadafina, L. Arcidiacono, S. Tavarini, C. Sammicheli, D. Laera, A. G. O. Manetti, et al. 2016. *Staphylococcus aureus*-dependent septic arthritis in murine knee joints: local immune response and beneficial effects of vaccination. *Sci. Rep.* 6: 38043.
47. Putnam, N. E., L. E. Fulbright, J. M. Curry, C. A. Ford, J. R. Petronglo, A. S. Hendrix, and J. E. Cassat. 2019. MyD88 and IL-1R signaling drive antibacterial immunity and osteoclast-driven bone loss during *Staphylococcus aureus* osteomyelitis. *PLoS Pathog.* 15: e1007744.
48. Briot, K., and C. Roux. 2015. Glucocorticoid-induced osteoporosis. *RMD Open* 1: e000014.
49. Luís, M., J. Freitas, F. Costa, F. Buttgereit, M. Boers, D. S. Jap, and T. Santiago. 2019. An updated review of glucocorticoid-related adverse events in patients with rheumatoid arthritis. *Expert Opin. Drug Saf.* 18: 581–590.
50. Fangtham, M., and A. N. Baer. 2012. Methicillin-resistant *Staphylococcus aureus* arthritis in adults: case report and review of the literature. *Semin. Arthritis Rheum.* 41: 604–610.
51. Hruz, P., A. S. Zinkernagel, G. Jenikova, G. J. Botwin, J. P. Hugot, M. Karin, V. Nizet, and L. Eckmann. 2009. NOD2 contributes to cutaneous defense against *Staphylococcus aureus* through alpha-toxin-dependent innate immune activation. *Proc. Natl. Acad. Sci. USA* 106: 12873–12878.
52. Deshmukh, H. S., J. B. Hamburger, S. H. Ahn, D. G. McCafferty, S. R. Yang, and V. G. Fowler, Jr. 2009. Critical role of NOD2 in regulating the immune response to *Staphylococcus aureus*. *Infect. Immun.* 77: 1376–1382.
53. O'Connor, O. A., M. Özcan, E. D. Jacobsen, J. M. Roncero, J. Trotman, J. Demeter, T. Masszi, J. Pereira, R. Ramchandren, A. Beaven, et al. 2019. Randomized phase III study of alisertib or investigator's choice (selected single agent) in patients with relapsed or refractory peripheral T-cell lymphoma. *J. Clin. Oncol.* 37: 613–623.
54. Roberts, A. E. L., K. N. Kragh, T. Bjarnsholt, and S. P. Diggle. 2015. The limitations of in vitro experimentation in understanding biofilms and chronic infection. *J. Mol. Biol.* 427: 3646–3661.
55. Oliveira, L. M., F. M. E. Teixeira, and M. N. Sato. 2018. Impact of retinoic acid on immune cells and inflammatory diseases. *Mediators Inflamm.* 2018: 3067126.
56. Dawson, H. D., G. Collins, R. Pyle, M. Key, and D. D. Taub. 2008. The Retinoic Acid Receptor-alpha mediates human T-cell activation and Th2 cytokine and chemokine production. *BMC Immunol.* 9: 16.
57. Iwata, M., Y. Eshima, and H. Kagechika. 2003. Retinoic acids exert direct effects on T cells to suppress Th1 development and enhance Th2 development via retinoic acid receptors. *Int. Immunol.* 15: 1017–1025.

58. Bai, A., N. Lu, H. Zeng, Z. Li, X. Zhou, J. Chen, P. Liu, Z. Peng, and Y. Guo. 2010. All-trans retinoic acid ameliorates trinitrobenzene sulfonic acid-induced colitis by shifting Th1 to Th2 profile. *J. Interferon Cytokine Res.* 30: 399–406.
59. Shi, X. N., H. Li, H. Yao, X. Liu, L. Li, K. S. Leung, H. F. Kung, and M. C. M. Lin. 2015. Adapalene inhibits the activity of cyclin-dependent kinase 2 in colorectal carcinoma. *Mol. Med. Rep.* 12: 6501–6508.
60. Ocker, M., C. Herold, M. Ganslmayer, E. G. Hahn, and D. Schuppan. 2003. The synthetic retinoid adapalene inhibits proliferation and induces apoptosis in colorectal cancer cells in vitro. *Int. J. Cancer* 107: 453–459.
61. Fu, Y., Y. Zhang, M. Gao, L. Quan, R. Gui, and J. Liu. 2016. Alisertib induces apoptosis and autophagy through targeting the AKT/mTOR/AMPK/p38 pathway in leukemic cells. *Mol. Med. Rep.* 14: 394–398.